Engineering Failure Analysis 150 (2023) 107277

Contents lists available at ScienceDirect

Engineering Failure Analysis

journal homepage: www.elsevier.com/locate/engfailanal

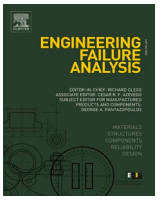

Analysis of Stochastic Matrix Crack Evolution in CFRP Cross-Ply Laminates under Fatigue Loading

Xi Li [a,b,*], Rinze Benedictus [a], Dimitrios Zarouchas [a,b]

[a] Faculty of Aerospace Engineering, Delft University of Technology, Kluyverweg 1, 2629HS Delft, the Netherlands
[b] Center of Excellence in Artificial Intelligence for Structures, Aerospace Engineering Faculty, Delft University of Technology, the Netherlands

ARTICLE INFO

Keywords:
In-situ damage monitoring
Phenomenological model
Fatigue
Composite laminates

ABSTRACT

The present work aims at understanding the stochastic matrix crack evolution in CFRP cross-ply laminates under tension–tension fatigue loading. An experimental campaign was carried out on twenty-three specimens at different stress levels, while two optical techniques were used for the in-situ monitoring of the accumulation of transverse matrix cracks. The results showed a significant scatter in crack evolution among specimens. This stochastic behaviour was further investigated using image analysis and numerical modelling. It was found that transverse matrix cracks can be classified into the independent and dependent cracks based on a critical crack spacing. Furthermore, the severity of interaction among cracks was quantified by introducing a dependent crack ratio. Finally, a strength-based probabilistic model was proposed to describe the scattering regime of the crack evolution. The agreement between model and test results indicates that local strength variations of 90 plies are the dominant scattering source governing the initial fatigue resistance to cracking and determining the accumulation of transverse matrix cracks among specimens. These results may provide a new insight into the stochastic nature of matrix cracking in composite laminates and aid in the design of fatigue resistance properties.

1. Introduction

Composite laminates undergo a progressive damage process during their service life [1,2]. When subjected to fatigue loading, a three-stage damage accumulation has been characterised for laminates, starting with matrix cracking, followed by delamination and ending with fibre damage [3–5]. Matrix cracking accumulates to a saturated state, also referred to the characteristic damage state [4,5], and the stiffness of the laminate can be reduced by 10–15% under fatigue loading [6]. While matrix cracking is the dominant damage mechanism during the early fatigue life, delamination between adjacent plies can be induced, further contributing to the stiffness degradation [7,8]. The progressive damage method, which typically includes a stress analysis model, a failure criterion and a material degradation model [9], has shown great potential and efficiency in predicting the mechanical response and damage assessment of laminated structures, such as the Type IV composite pressure vessels reported in [10]. However, the interaction, synergy and sometimes even competition, between similar and different damage mechanisms of laminates under fatigue loading, are yet on the way to be fully explored from experiments and further considered in the predictive modelling. In the effort to establish a physical/physics-based fatigue damage framework, the focus should first be put on understanding and classifying the matrix crack accumulation process [1].

* Corresponding author at: Faculty of Aerospace Engineering, Delft University of Technology, Kluyverweg 1, 2629HS Delft, the Netherlands.
E-mail address: Xi.Li@tudelft.nl (X. Li).

https://doi.org/10.1016/j.engfailanal.2023.107277
Received 27 February 2023; Received in revised form 18 April 2023; Accepted 22 April 2023
Available online 28 April 2023

The generation of off-axis matrix cracks is a stochastic process that exhibits both temporal and spatial variations [3,11]. This phenomenon has been extensively studied and it has been found that defects in the local microstructure of off-axis plies, *i.e.* matrix porosity, debonded fibre, local volume fraction of fibre and matrix, and their spatial distribution, affect when and where an off-axis crack initiates [12]. Due to the current manufacturing processes, these local defects are difficult to control [13–15], thus posing a challenge to elucidate the mechanisms of off-axis crack initiation. Efforts have been made to quantify the stochastic fibre architectures and defects by using image analysis techniques; based on this, representative volume element models have been developed which provide the link between the microstructure and the local material property [12,16,17]. Accordingly, the randomness of crack initiation caused by the variations in local microstructures at off-axis plies can be related to the variations in local material properties.

So far, strength-based or energy-based approaches [18,19] have been used in probabilistic crack evolution models, with the variations in local strength or local fracture toughness introduced. The strength-based approach checks whether the local stress reaches the material strength, while the energy-based approach checks whether the energy release rate in the front of a microcrack (or flaw) reaches the local fracture toughness [20]. Although the energy-based approach could consider the effect of ply thickness [21], the size and the pattern of the micro-cracks need be accurately obtained to determine the variations in local fracture toughness [20]. Instead, the variations in local strengths at off-axis plies involved in the strength-based approach can be obtained directly by performing tensile tests on unidirectional lamina. However, it excludes the in-situ effect of off-axis strength and cannot be adapted to predict high-density crack evolution. Furthermore, band models have been proposed by discretising the off-axis plies of laminates into multiple elements to capture the distribution of in-situ local strengths in one/few tensile tests [22,23].

Probabilistic strength-based models have demonstrated the ability to describe the stochastic evolution of off-axis matrix cracks at both low and high densities under fatigue loading. For low density cracks, the model takes into account a statistical distribution of the local strengths at off-axis plies [24], which can be correlated with the statistical distribution of fatigue life for the crack initiation at different local regions, based on the Strength Life Equal Rank Assumption (SLERA) named by Chou and Croman [25]. SLERA states that a specimen should have the same probability within the statistical distributions of static strength, fatigue life and residual strength [26,27], considering that specimens with higher static strength have longer fatigue life [28,29]. Consequently, an ordered correlation can be established between the static strength and the fatigue life statistics [29]. Sendeckyj [30] used the SLERA to determine Weibull distribution parameters of static strength by converting fatigue data to equivalent static strength values. In the case of the high crack density, the model takes into account not only the local strength variation but also the stress redistribution around the cracked region [6,31,32], as both the local strength and the stress state of the off-axis plies determine the fatigue cycles to initiate a new matrix crack. By assuming that fatigue failure occurs when the residual strength is reduced to the value of the maximum applied stress, residual strength models as reviewed in [33], could be used to calculate the fatigue life for the crack initiation at the stress-redistributed region. As for the local stresses in the cracked region, they can be obtained by using different analytical and numerical methods. Analytically, shear lag analysis and variational analysis are two of the widely used methods, and the latter can take into account the stress transfer due to out-of-plane shear loading [34]. Based on finite element (FE) modelling, various techniques have been developed to simulate cracks in composites and to obtain redistributed stresses in the cracked region. Teimouri *et al.* [35] found that trilinear cohesive element models were more accurate than the bilinear models when fibre bridging effects were considered. Karimi *et al.* [36] proposed an adaptive virtual crack closure technique that can significantly improve the accuracy of fatigue crack growth simulation. Garoz *et al.* [34] predicted the local stresses of a cracked laminate by applying the seam crack technique in a representative unit cell to duplicate the nodes at the crack surface.

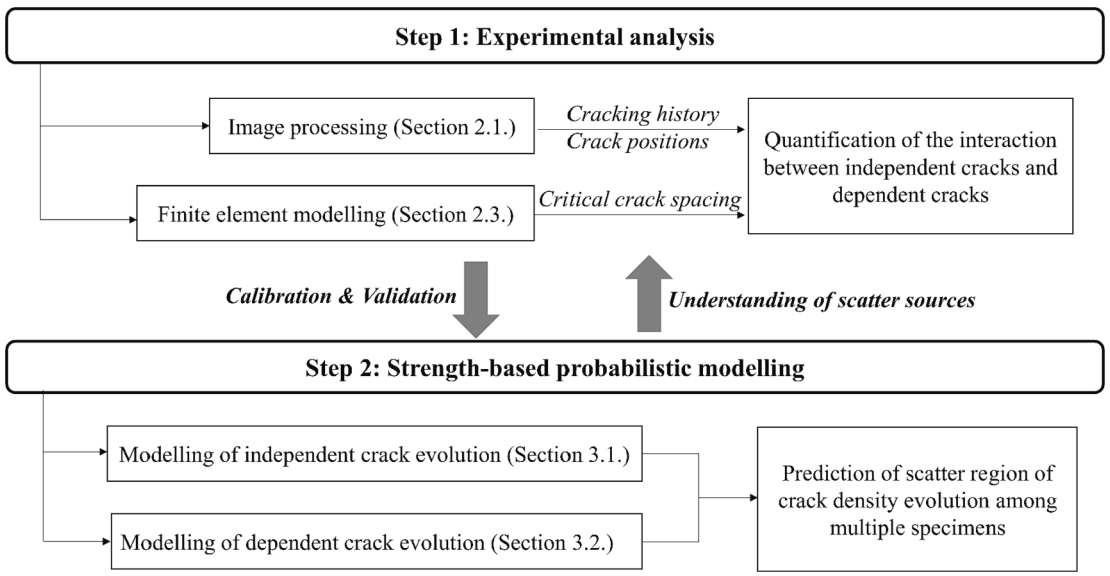

Fig. 1. Research scheme of present work.

Despite the efforts to understand the matrix crack evolution during fatigue loading using the probabilistic modelling, there are still open questions that this work attempts to address: how to model the stochastic matrix crack evolution over multiple specimens at different stress levels; how to quantify the interaction between adjacent matrix cracks; and how to consider the effect of delamination on matrix crack accumulation. As observed in our previous experimental work [3], for carbon/epoxy cross-ply laminates, the evolution of transverse matrix cracks during the early fatigue life varies significantly among specimens with a similar stiffness degradation trend. Specifically, the saturated crack density varies from ~ 0.2 to 0.4 mm^{-1} among specimens. For specimens with lower saturated crack densities, more fatigue cycles are consumed to reach the saturation of transverse matrix cracks [3]. Considering that each specimen has certain strength variations in the local region of 90 plies, these strength variations should determine the initial fatigue resistance to the matrix cracking, as reported by Pathakokila *et al.* [37] as a source of scatter in fatigue data among specimens. It could also affect the accumulation and interaction of transverse matrix cracks. Therefore, a strength-based probabilistic framework is proposed in this paper so as to further investigate and better understand the experimental results as reported in [3].

Overall, the objective of this work is to understand the stochastic evolution of transverse matrix cracks among specimens tested under tension–tension fatigue loading. Fig. 1 shows the structure of the present work, including both experimental and modelling aspects. First, the interaction among transverse matrix cracks was analysed and quantified based on the test data and finite element analysis. Then, a strength-based probabilistic model, taking into account the variations in local strengths at 90 plies, was established to predict the scattering range of crack density evolution among multiple specimens. Later, after validation by experimental results, the model was used to uncover the scatter sources of crack evolution from specimen to specimen.

2. Experimental analysis

2.1. Specimen preparation and test set-up

The ply configuration of the specimens is $[0_2/90_4]_s$, and they were obtained from several laminated panels (300 × 300 mm) made with the unidirectional prepreg Hexply® F6376C-HTS(12 K)-5–35% with a nominal thickness of 0.125 mm. Curing was performed at 177 °C and 7 bar for two hours, as recommended by the manufacturer [38]. The specimens were subjected to cyclic tension–tension loading with constant amplitude of sinusoidal waves was applied to the specimens. The stress ratio was set at 0.1 to reduce the time cost of fatigue testing, as matrix cracks accumulate more rapidly at lower stress ratios [5]. The frequency was set at 5 Hz to avoid self-heating of the laminate under cyclic loading. Five different stress levels were considered in this work, with the maximum cyclic stress at 74%, 70%, 66%, 63% and 55% of the Ultimate Tensile Strength (UTS) of the $[0_2/90_4]_s$ laminate, where 55% of UTS was used to generate the P-S-N curves. The above-mentioned percentages of UTS represent the stress level of the whole laminate, but not the stress level of 90 plies within the cross-ply laminate, as the tensile strength of 90 plies is much lower than the ultimate tensile strength of the laminate. Based on the axial stress (σ_{90i}) of the laminate at the onset of the first transverse crack at 90 plies, as measured under static loading [11], the corresponding stress levels at 90 plies can be obtained by the percentages of the maximum cyclic stress to the σ_{90i}. In Table 1, the case with the percentages of σ_{90i} greater than 100% indicates the initiation of transverse matrix cracks on the first cycle

Table 1
Summary of tested specimens included in the present work (Specimen ID: stress level - specimen number; G1 - Group 1; G2 - Group 2.

Specimen ID	Maximum cyclic stress $\bar{\sigma}_{applied}$ (MPa)	Percentage of UTS (%)	Percentage of σ_{90i} (%)	Group of stiffness degradation	Cycles for saturation of transverse matrix cracks	Saturated crack density (mm^{-1})	Delamination ratio at saturation of transverse matrix cracks
S1-1	533	74	105	G1	10,500	0.2625	0.0012
S1-2	533	74	105	G1	17,000	0.2250	0.0299
S1-3	533	74	105	G2	28,500	0.2563	0.0931
S2-1	507	70	99	G1	28,000	0.2658	0.0293
S2-2	507	70	99	G1	32,000	0.2143	0.1147
S2-3	507	70	99	G1	20,500	0.3497	0.0002
S2-4	507	70	99	G1	26,500	0.2911	0.0204
S2-5	507	70	99	G2	53,500	0.2166	0.1465
S2-6	507	70	99	G2	42,000	0.3474	0.0205
S2-7	507	70	99	G2	50,000	0.2656	0.0567
S3-1	480	66	94	G1	53,000	0.2750	0.0443
S3-2	480	66	94	G1	50,000	0.2938	0.0176
S3-3	480	66	94	G1	72,500	0.2625	0.1524
S3-4	480	66	94	G1	48,500	0.3500	0.0059
S3-5	480	66	94	G2	85,500	0.3125	0.0527
S3-6	480	66	94	G2	113,500	0.2125	0.1225
S4-1	453	63	89	G1	170,500	0.2405	0.1219
S4-2	453	63	89	G1	116,000	0.3822	–
S4-3	453	63	89	G1	118,500	0.3360	0.0148
S4-4	453	63	89	G2	220,000	0.3019	0.0309
S5-1	400	55	78	–	–	–	–
S5-2	400	55	78	–	–	–	–
S5-3	400	55	78	–	–	–	–

under fatigue loading. Conversely, the initiation of transverse matrix cracks occurs after certain fatigue cycles when the percentage of σ_{90i} is less than 100%.

Fig. 2(a) shows the experimental setup, where two pairs of cameras were used to measure the stiffness degradation and to monitor the damage evolution of the specimens in situ, as described in [3,39]. One pair of 9 megapixel cameras was used to capture the cracks along each edge of the specimens. The edge surfaces of each specimen were covered with thin white paint in order to enhance the white-black contrast of cracked and uncracked regions. A user-defined algorithm [11] was then developed to automatically identify and locate the transverse matrix cracks on the 90 plies using image processing, which has been recognised as an efficient method for the in-situ crack monitoring of composite laminates under fatigue loading [40,41]. In this algorithm, the image was first processed by the bottom-hat filtering to compute the morphological closing of the image, followed by conversion to the binary image and noise reduction for subsequent crack labelling. As a result, the crack density can be obtained as the average number of transverse matrix cracks at both edges divided by the gauge length (~80 mm). In addition, another pair of 5 megapixel cameras was placed in the front to measure the deformation of the specimens using the Digital Image Correlation (DIC) technique [42]. The length of the gauge region is ~80 mm for edge observation and DIC analysis. Every 500 cycles, a tensile unloading-loading ramp was applied in a two-second period (see Fig. 2(b)), and both pairs of cameras were triggered synchronously to capture images every 50 ms or 200 ms. Table 1 lists the details of the specimens tested at different stress levels.

2.2. Test results

As reported in the literature [3–5], a three-stage stiffness degradation in a rapid-slow-rapid manner is representatively behaved by composites under fatigue loading. Our work focuses on the first rapid stage (Stage I), where a significant loss of stiffness occurs within a short period of time due to the formation of transverse matrix cracks and delamination. Therefore, almost all tests were run until the stiffness degradation had passed through Stage I and approached a stable phase, or the number of fatigue cycles had reached a run-off of 1E+06 cycles.

The axial modulus of the specimens was measured from the slope of the axial stress and average axial strain measured by DIC for each tensile loading ramp after every 500 cycles. Fig. 3 plots the degradation trends of the normalised axial modulus E_N/E_0 as the number of fatigue cycles increases. Here, E_0 and E_N are the axial modulus at the initial state and the N^{th} cycle, respectively. As observed, the E_N/E_0 at the plateau approaches that of the ply discount model, which assumes zero value for the transverse modulus E_{22}

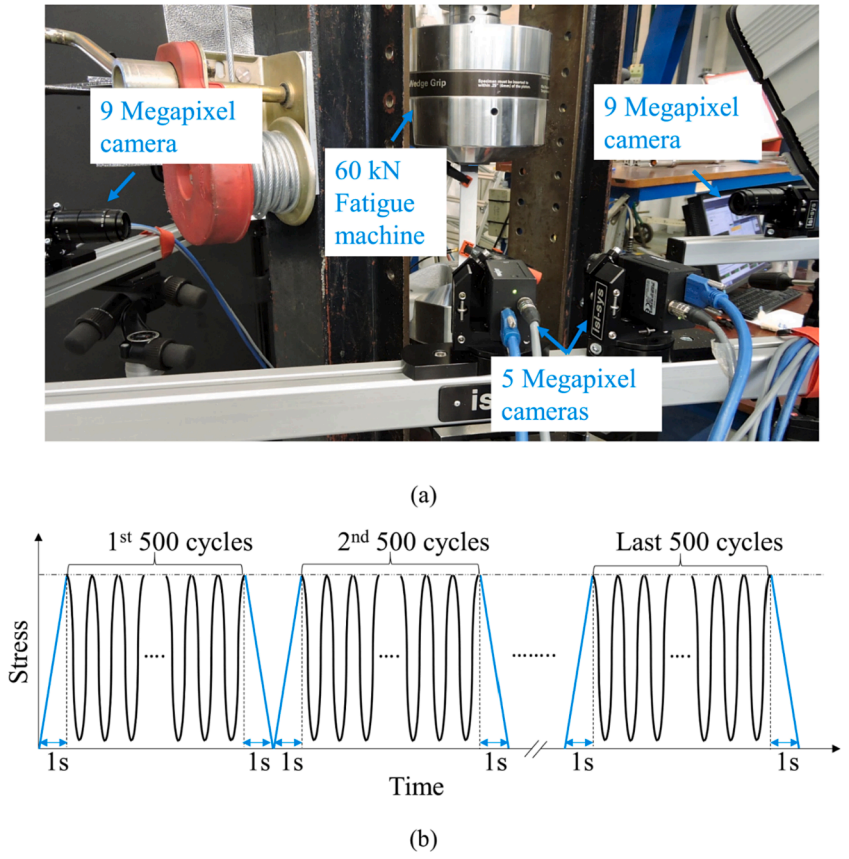

Fig. 2. Test set-up (a) and loading profile (b) of fatigue tests.

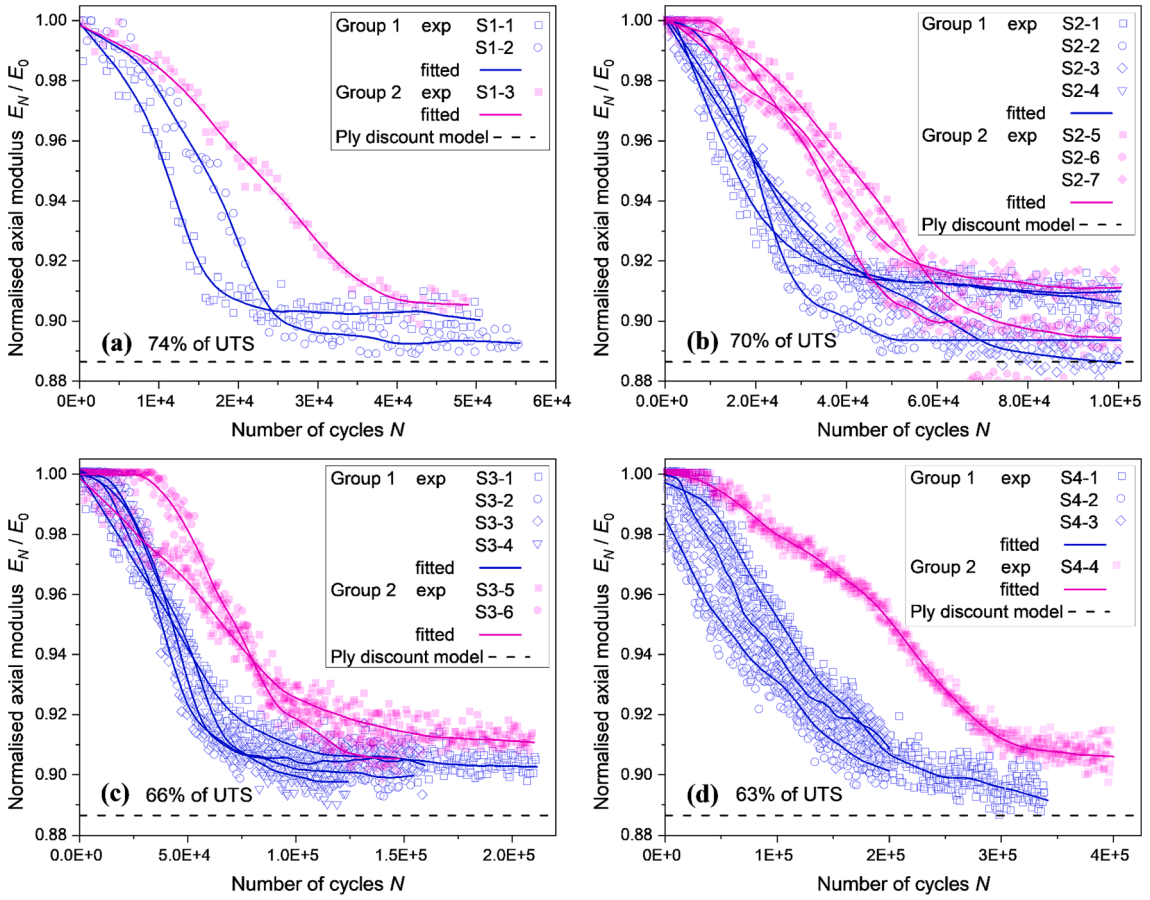

Fig. 3. The decreasing of normalised axial modulus with the increase of fatigue cycles under different stress levels: (a)74% of UTS; (b)70% of UTS; (c) 66% of UTS; (d) 63% of UTS.

and the in-plane shear modulus G_{12} in the 90 plies. This indicates that the stiffness degradation of most specimens approaches the second stage before the end of the test. Furthermore, the specimens can be divided into two groups for all stress levels, based on the rate of stiffness degradation within the first stage. Group 1 specimens show a faster degradation trend than that Group 2 specimens (see Fig. 3). This is due to the manufacturing inhomogeneity which results in different levels of fatigue resistance among specimens.

During the fatigue test, most of the transverse matrix cracks propagated through the entire width of the laminate within 500 cycles, and axial strain concentration stripes were produced on the outer 0 ply along with the generation of new cracks, as shown in Fig. 4. Red arrows indicate the location of the new cracks. While the evolution of transverse matrix cracks is scattered within each group of specimens (see dot plots in Fig. 12 and Fig. 13), transverse matrix crack saturation was reached later for specimens with lower saturated crack density (see Table 1). It was also observed that delamination started during the accumulation of transverse matrix cracks. Fig. 4(b) shows the damage at 90 plies and 0/90 interfaces from the edge view as the transverse matrix cracks saturated. The specimen with the lowest saturated crack density (top) in Group 1 and the specimen with the highest saturated crack density (bottom) in Group 1 are shown for each stress level. As can be seen from Table 1 and Fig. 4(b), for each group of specimens with a similar trend of stiffness degradation within Stage I, the specimen with the higher saturated crack density grew less delamination grew. Apparently, both damage mechanisms compete to contribute to the stiffness degradation and energy dissipation that are similar for each group of specimens under the constant load or displacement in a linear-elastic material system. Therefore, there are different levels of interaction (competition) between transverse matrix cracking and delamination among specimens in each group. As a result, a significant scatter in crack accumulation is presented for each group of specimens, with the saturated crack density at 90 plies (nominal thickness: 1 mm) in the range of ~ 0.2 to 0.4 mm^{-1}, irrespective of the applied stress level.

2.3. *Characterisation of independent and dependent cracks*

Off-axis matrix cracks with high local density tend to interact with their neighbours, resulting in local stress redistributions [6,24,31,43]. To quantify the level of interaction between adjacent matrix cracks, it is necessary to classify independent (non-interactive) cracks and dependent (interactive) cracks: the former are located far from neighbours where the local stress remains at a uniform stress level within the 90 plies, whereas the latter initiate close to existing cracks, where a redistributed stress state exists.

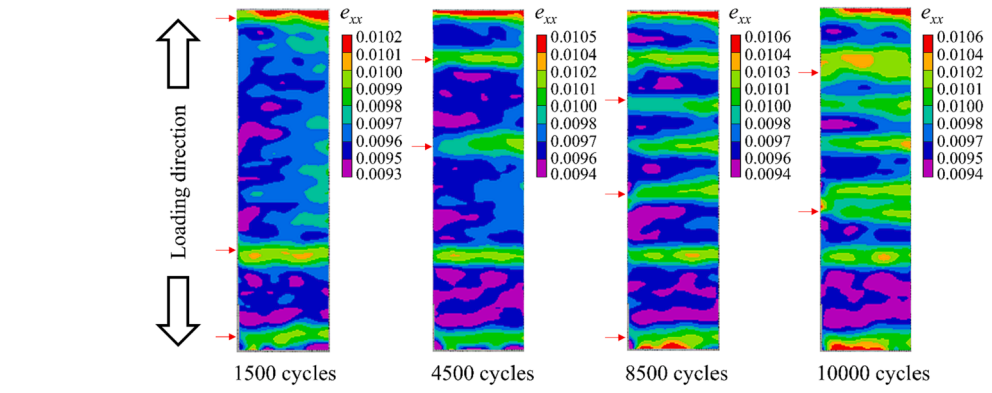

(a)

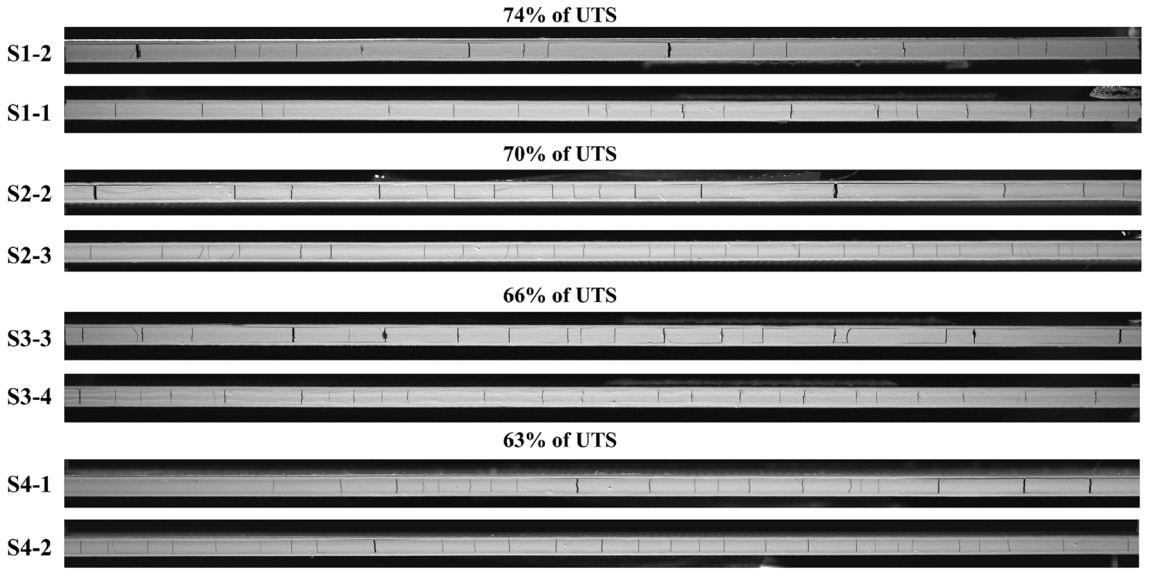

(b)

Fig. 4. Axial strain concentration at the exterior 0 ply for the specimen S2-2 under the stress level at 70% of UTS (a); Images at the gauge region from the edge view when transverse matrix cracks saturate, for the specimen with the lowest saturated crack density at Group 1 (top) and for the specimen with the highest saturated crack density at Group 1 (bottom) under each stress level (b).

2.3.1. Finite element modelling

To determine whether a transverse matrix crack is independent or dependent, a critical crack spacing should be determined. For the given cross-ply configuration, a parametric finite element analysis was performed to calculate the local stress state between two cracks at different distances and to obtain the critical crack spacing.

As shown in Fig. 5(a), a two-dimensional model with a length of 10 mm was built from the edge view using CPE4R (reduced 4-node bilinear plane strain quadrilateral) elements. The mesh size was set to 0.05 mm based on a sensitivity analysis. The linear-elastic material properties of the unidirectional lamina, as listed in Table 2, were assigned to the model. To simulate the orthotropic feature, local material coordinates with orientations of 0° and 90° were set to 0 and 90 plies, respectively. For the cracked region, seam cracks were applied at the red locations marked in Fig. 5(a). In ABAQUS, a seam crack defines an edge or a surface with overlapping nodes that can separate during an analysis [44]. The transition of the nodes at the left end of the model was constrained along the loading direction. The force was applied to a reference point coupled to all nodes at the right end of the model, as shown in Fig. 5(a). Considering that each transverse matrix crack is assumed to occur at the loading phase during a sinusoidal cycle, the force applied on the reference point in the model can be simplified by introducing a linearly increasing force up to the maximum cyclic load. Based on the experimental observation, delamination usually initiates and propagates in the low crack density region where crack interaction rarely occurs. In addition, delamination can have a limited effect on the stress field along the in-plane tensile load. Therefore, a perfect bond at 0/90 interfaces, as indicated by the black lines in Fig. 5(a), has been set in the current model. The effect of the length of the model has been checked and it is found that there is no difference in the modelling results of the local stress state at the cracked region from the model with a length above 10 mm.

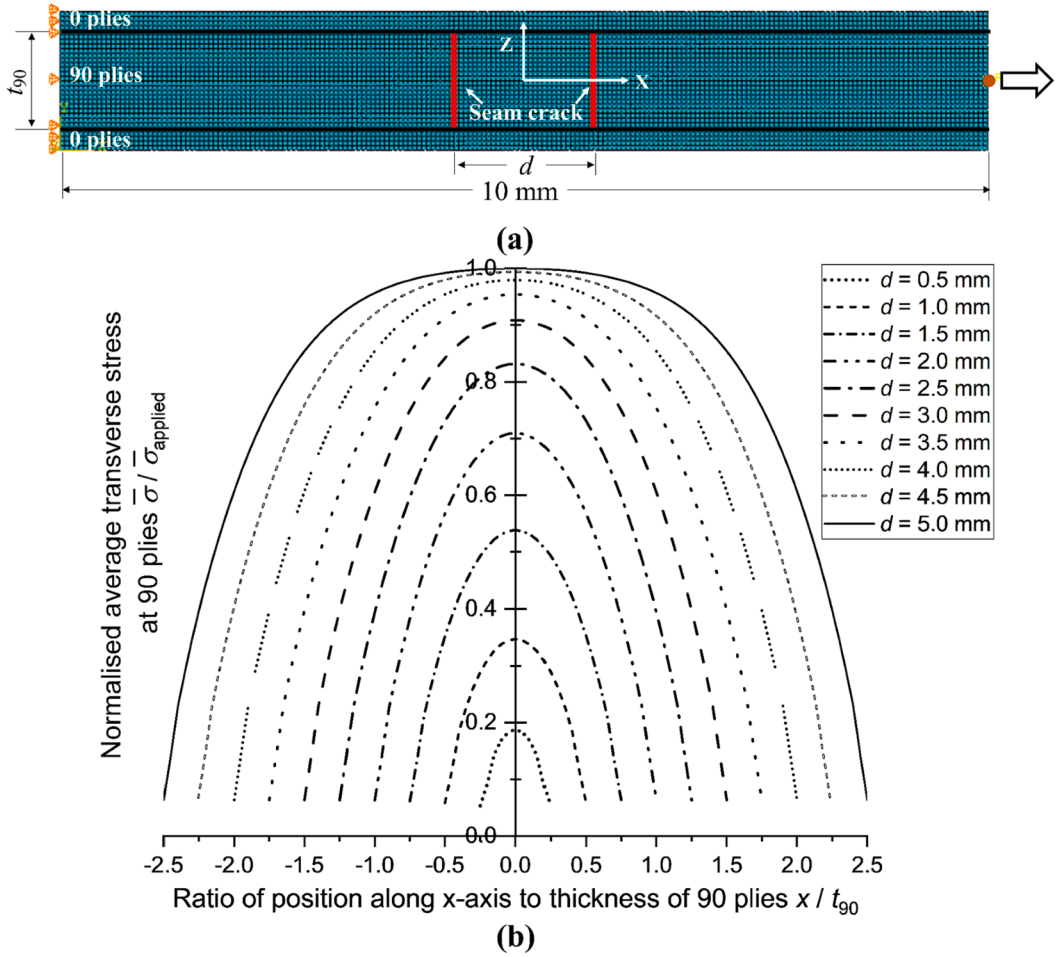

Fig. 5. Schematic diagram of the finite element model for a cracked laminate, including boundary and loading conditions, ply configuration and geometry dimensions (a); The normalised average transverse stress at 90 plies $\overline{\sigma}/\overline{\sigma}_{applied}$ versus ratio of position along x-axis between two transverse matrix cracks to thickness of 90 plies x/t_{90} (b). (d - crack spacing; t_{90}- thickness of 90 plies).

Table 2
Input material properties for the finite element model [3].

Material properties	Values
Longitudinal modulus	$E_{11} = 142$ GPa
Transverse modulus	$E_{22} = E_{33} = 9.1$ GPa
In-plane shear modulus	$G_{12} = G_{13} = 5.2$ GPa
Transverse shear modulus	$G_{23} = 3.5$ GPa
In-plane Poisson ratio	$\nu_{12} = \nu_{13} = 0.27$
Transverse Poisson ratio	$\nu_{23} = 0.30$

2.3.2. Critical crack spacing

Fig. 5(b) shows the axial normal stress state at 90 plies between two cracks with a spacing varying from 0.5 mm to 5 mm. Here, the axial stress state is averaged along the thickness, denoted as $\overline{\sigma}$, and then normalised by the maximum cyclic stress applied at 90 plies $\overline{\sigma}_{applied}$. In other words, $\overline{\sigma}_{applied}$ is the ply stress at 90 plies for cases without cracks. The x-axis in Fig. 5(b) is the ratio of the position between the two cracks, X, to the 90-ply thickness, t_{90}, of the $[0_2/90_4]_s$ laminate. As observed, the axial stress at the centre of the two cracks gradually converges to the applied level as the crack spacing d increases. Here, the critical case can be considered to be that at $d = 4.5$ mm, where the $\overline{\sigma}/\overline{\sigma}_{applied}$ at the centre of the two cracks is very close to that at $d = 5.0$ mm, with a difference of less than 0.001. Consequently, the average axial stress at the centre of the two cracks is lower than the applied level when the crack spacing is less than 4.5 mm. This observation indicates that the overlap of stress perturbation between two cracks starts at a distance less than 4.5 mm, and the driving force to initiate a new crack in between is affected by the occurrence of previous cracks. In the case of $d \geq 4.5$ mm, the average axial stress is equal to the applied level at the centre of the two cracks, where the new crack does not interact with its

neighbours. Therefore, the critical crack spacing is found to be 4.5/2 = 2.25 mm.

2.3.3. Dependent crack ratio

Having estimated the critical crack spacing, the dependent and independent transverse matrix cracks generated in the ~80 mm gauge region can be grouped accordingly. The maximum number of independent cracks T_a at the saturation state scatters in a certain range, as summarised in Fig. 6(a). The mean value of T_a is 17 (see the blue dashed line). In addition, a dependent crack ratio r_d is introduced to represent the proportion of dependent cracks generated in one specimen. It is calculated as the maximum number of dependent cracks T_b divided by the maximum number of independent cracks T_a. As shown in Fig. 6(b), the dependent crack ratio r_d ranges from 0.1 to 0.7 at the saturation state. A larger dependent crack ratio is produced for the specimen with a higher saturated crack density, which is usually associated with less delamination growth at the saturation state of transverse matrix cracks, as mentioned in Section 2.2. In other words, when strong interaction among transverse matrix cracks occurs in a specimen, it is accompanied by weak interaction between transverse matrix cracks and delamination. By assuming that the maximum number of independent cracks is constant at 90 plies, which in this case is 17, the competition between transverse matrix cracks and delamination found in Section 2.2 can be further related to the competition between dependent cracks and delamination. Here, the assumption of a constant T_a (maximum number of independent cracks) is used to simplify the stochastic generation of transverse matrix cracks. As a result, in the analysis of crack evolution, the severity of the interaction among transverse matrix cracks as well as the interaction between transverse matrix cracks and delamination can be quantified by the dependent crack ratio proposed here: a large dependent crack ratio represents strong interaction among cracks as well as weak interaction between transverse matrix cracks and delamination, and vice versa.

3. Probabilistic modelling

A strength-based probabilistic model is developed hereafter to describe the stochastic accumulation of transverse matrix cracks under fatigue loading. This strength-based model contains two parts: one is the modelling of independent crack accumulation in a non-interactive scheme (see Section 3.1) and the other is the modelling of dependent crack accumulation in an interactive scheme (see Section 3.2). Both parts require data input from fatigue tests at stress levels of 70%, 63% and 55% of UTS to calibrate the associated empirical parameters. In Section 3.3, the model is validated using crack evolution measured from tests at stress levels of 74% and 66% of UTS. The purpose is to gain a better understanding of the ability of the model to mimic the crack evolution.

3.1. Independent crack accumulation

Since the initiation of independent cracks depends mainly on the local strength of 90 plies, it is necessary to obtain the statistical distribution of local strengths and then relate the local strength to the fatigue life of independent crack initiation.

3.1.1. Collection of local strength at 90 plies

In order to obtain the local strength variations of 90 plies, the matrix crack evolution was monitored during static tests at a loading rate of 1 mm/min on five specimens, following the experimental methods reported in [11]. The generated independent cracks were then identified by the critical crack spacing as presented in Section 2.3.2. When the independent cracks initiated under tensile loading, the applied axial stresses of the laminates were used to calculate the transverse stresses at 90 plies, and the residual thermal stresses were not included in the present study. These stresses can later be considered as the local strengths of 90 plies S shown in Fig. 7. A Weibull distribution, with the probability density function shown in Eq. (1), was then used to fit the local strengths S collected from

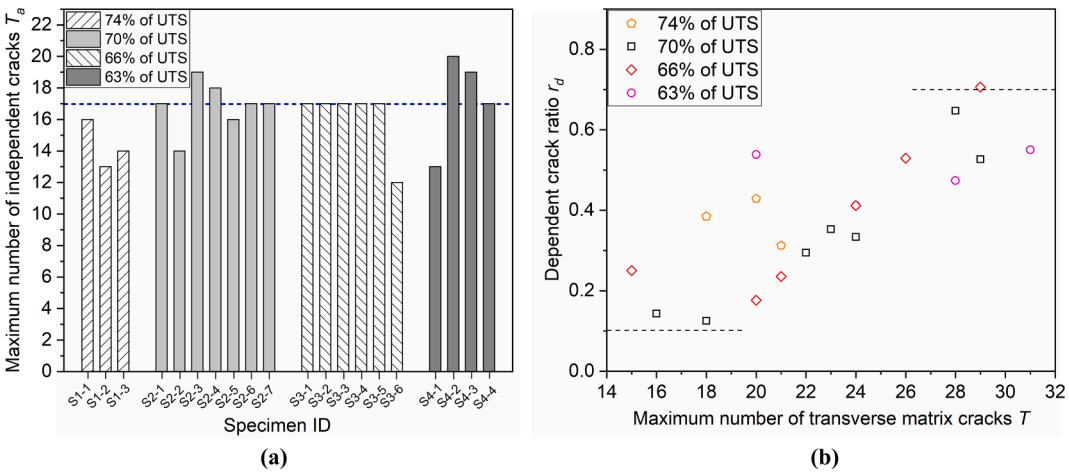

Fig. 6. The maximum number of independent cracks (a), and the dependent crack ratio versus the maximum number of cracks (b) at the saturation state of transverse matrix cracks under different stress levels.

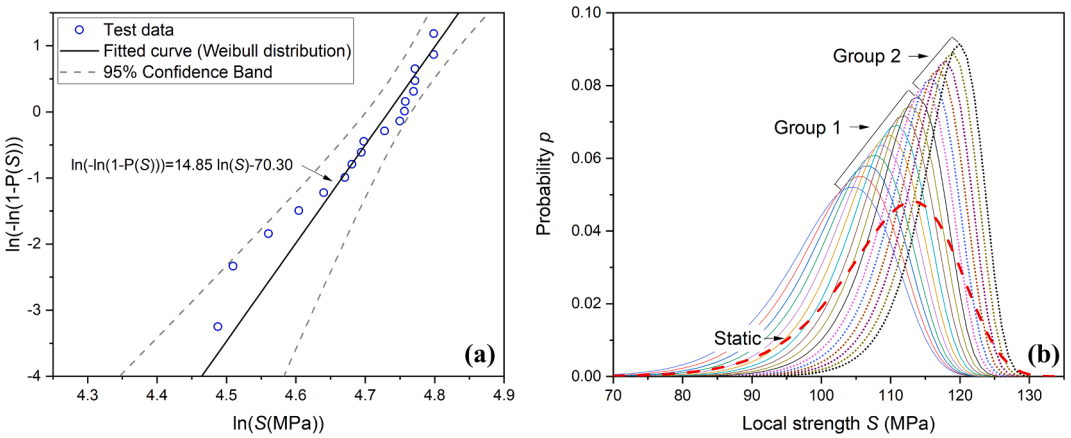

Fig. 7. Weibull parameter determination of test data collected under static tensile loading, where $P(S)$ is the cumulative probability of local strength S (a); Two groups of Weibull distributions (scale factors ($\eta \in$ [105 MPa, 120 MPa]) and shape factors ($\beta \in$ [14.85, 29.85])) about the local strengths of 90 plies generated based on the Weibull distribution collected from static tests (red dash line) (b). (For interpretation of the references to colour in this figure legend, the reader is referred to the web version of this article.)

five samples. The determination of the Weibull parameters on the logarithmic axis is plotted in Fig. 7(a). As observed, the scale factor η is 113.72 MPa and the shape factor β is 14.85.

$$p(S) = \begin{cases} \frac{\beta}{\eta}\left(\frac{S}{\eta}\right)^{\beta-1} e^{-\left(\frac{S}{\eta}\right)^{\beta}}, S \geq 0 \\ 0, S < 0 \end{cases} \tag{1}$$

This Weibull distribution (see the red dashed line in Fig. 7(b)) represents the local variation in strength for 90 plies across all specimens tested under fatigue loading.

3.1.2. *Local strength - fatigue life relation*

The number of cycles N_a for independent cracks initiation was also measured during fatigue testing at 70% of UTS. It was then fitted by a Weibull distribution (η: 13554.41; β: 1.18). In addition, the Strength Life Equal Rank Assumption (SLERA) [25] is applied here and its applicability is discussed in Section 4. According to SLERA, each pair of local strength S_a (unit: MPa) and fatigue life N_a was correlated with the same cumulative probability of independent crack initiation, as expressed by:

$$S_a = 53.36408 \times N_a^{0.07952} \text{ (at 70\% of UTS)} \tag{2}$$

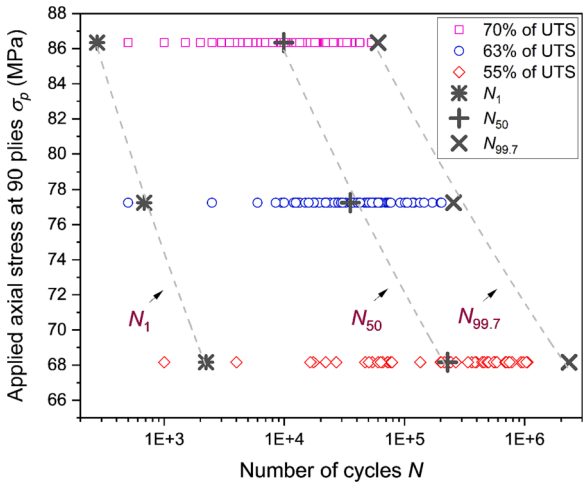

Fig. 8. Scatter of fatigue life related to the initiation of independent cracks collected from fatigue test under three different stress levels, and the fitted P-S-N curves. (Note: the black markers indicate the fatigue life at cumulative probabilities of 1%, 50% and 99.7% for the statistical distributions of fatigue life related to independent crack initiation under the different stress levels.).

However, Eq.(2) is limited to determining the fatigue life N_a given a local strength S_a at the 70% UTS stress level. To extend this local strength - fatigue life relationship from the 70% of UTS stress level to other stress levels, the number of cycles N_a required for independent crack initiation was also measured at the 63% and 55% of UTS stress levels. P-S-N curves can then be plotted at the 1%, 50% and 99.7% cumulative probabilities, based on the statistical distributions of fatigue life in terms of independent crack initiation at the 70%, 63% and 55% UTS stress levels, as shown in Fig. 8. The black markers in Fig. 8 for each stress level represent the fatigue life N_1, N_{50}, $N_{99.7}$ with the cumulative probabilities of 1%, 50% and 99.7% respectively. Based on the P-S-N curves, the relationship between the applied stress level σ_{pi} and the fatigue life to initiate an independent crack N_a is established by Basquin's power law equation:

$$\sigma_{pi} = A \times N_a^B \tag{3}$$

where B is set to -0.0647, which is the slope of the P-S-N curve at the 99.7% cumulative probability; A can be derived in the combination with Eq.(2). In this way, if a local strength S_a is known, the number of cycles N_a to initiate an independent crack at any stress level σ_{pi} can be calculated.

3.1.3. Fatigue life of independent crack initiation

Having obtained the local strength - fatigue life relationship, the next step is to describe the differences in local strength variation among specimens, after which the scatter of independent crack evolution as a function of fatigue cycles can be modelled.

For specimens with lower initial fatigue resistance to cracking (more cracks at the saturation state), more significant manufacturing-induced inhomogeneity is presented, which could contribute to a low average local strength of 90 plies with a wide scatter band. The opposite should be true for specimens with higher initial fatigue resistance to cracking. Accordingly, a variety of Weibull distributions, based on the reference distribution of local strengths from static tests (see the red dashed line in Fig. 7(b)), can be generated to represent different variations in local strengths at 90 plies and different initial fatigue crack resistance from specimen to specimen. As shown in Fig. 7(b), for Weibull distributions positioned along the x-axis, both scale factors ($\eta \in$ [105 MPa, 120 MPa]) and shape factors ($\beta \in$ [14.85, 29.85]) increase monotonically, and the higher peak is accompanied by a narrower spread band. Here, the scale factors are scattered around 113.72, which is the same as the scale factor of the Weibull distribution from the static tests (see Section 3.1.1). It indicates the local strength with the highest probability of all the specimens. The shape factors should be greater than 14.85 which is the shape factor of the Weibull distribution from static tests and represents the dispersion of local strengths across all specimens. The reason for this is that the dispersion of local strengths of one specimen should be equal to or less than that of all specimens. Finally, the range of scale and shape factors that could significantly affect the upper and lower limits of the scatter region of the crack density evolution during the early fatigue cycles, is calibrated based on the modelling results of independent crack evolution as described below.

Using a generated distribution of local strengths (see Fig. 7(b)) as an input, the statistical distribution of fatigue life for independent crack initiation at a given stress level can be obtained according to Eq. (2) and Eq. (3). The associated cumulative probability of this fatigue life distribution for an arbitrary cycle can be regarded as the probability of independent crack initiation at that cycle. The maximum of the cumulative probability was set at 0.997 to avoid the infinite fatigue life. Then, by assuming that the total number of independent cracks at the saturation T_a is constant, the number of independent cracks can be modelled as a function of fatigue cycles. Here, T_a is set to 17, which is the average of the specimens from the fatigue tests (see Fig. 6(a)). Fig. 9 shows the correlation between modelling and test results for independent crack accumulation at stress levels of 70% and 63% of UTS. This correlation validates the range of scale and shape factors and the grouping of the generated Weibull distributions shown in Fig. 7(b). Thus, these two groups of generated Weibull distributions adequately reflect the local variations at 90 plies for the two groups of specimens with different trends

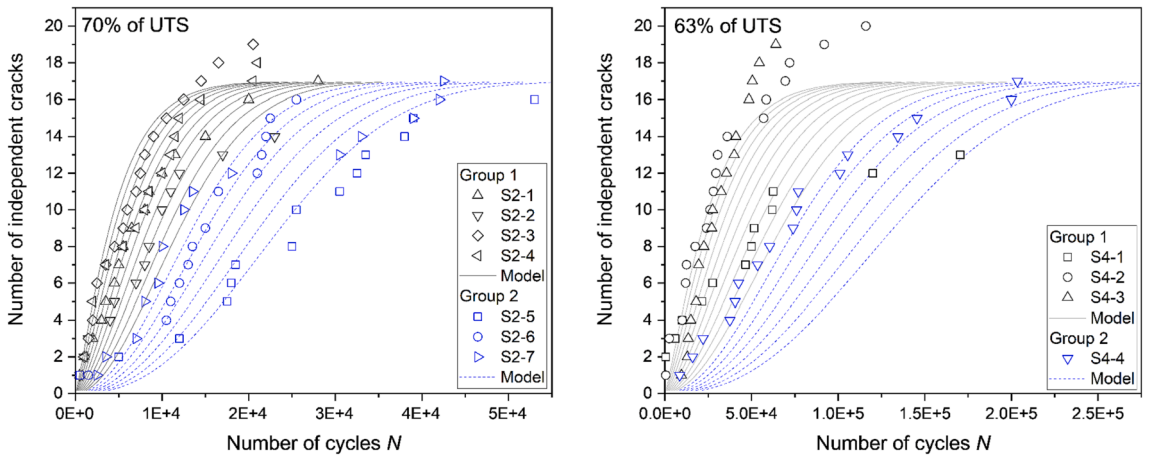

Fig. 9. Comparison between the experimental and modelling results about the evolution of independent cracks as a function of fatigue life under the stress levels at 70% and 63% of UTS.

of stiffness degradation trends (see Fig. 3).

3.2. Dependent crack accumulation

The initiation of dependent cracks is controlled both by the local strength of the 90 plies and by variations in the stress state around the independent cracks. In order to describe the accumulation of dependent cracks in the model, their interaction with independent cracks had to be clarified.

3.2.1. Severity of interaction

As the maximum number of independent cracks T_a is constant in the model, the dependent crack ratio r_d can be assigned to each generated Weibull distribution (see Fig. 7(b)). In this way, the severity of the crack interaction was determined from specimen to specimen. In Section 2.3.3., it was found that r_d ranges from 0.1 to 0.7 and it increases with the decrease in fatigue resistance to cracking. Based on these observations, a Weibull distribution of local strengths (in Fig. 7(b)) at each group is matched with a dependent crack ratio r_d such that r_d decreases proportionally from 0.7 to 0.1 as the peak of the Weibull distribution increases. As a result, the maximum number of dependent cracks T_b can be determined: $T_b = r_d \times T_a$.

3.2.2. Interactive region

Once the maximum number of dependent cracks T_b is known, interactive regions can be created in the model by matching dependent cracks with independent cracks. Due to the relatively low crack density in the present study, the crack interaction is less severe and complex compared to the very high density cases. As a result, it is not common for new cracks to form close to the previous dependent cracks at a distance less than the critical crack spacing. Therefore, a one-time interaction is considered, which means that an interactive region contains one pair of independent and dependent cracks.

To obtain the number of fatigue cycles that a dependent crack will initiate, the local strength S_a for the independent crack, the local strength S_b for the dependent crack and the crack spacing d must be determined. The following steps illustrate the collection and matching of S_a, S_b, and d for all interactive regions in a specimen.

Step1: The local strength $S_a(i)$ for the i^{th} independent crack is collected at the cumulative probability of the selected Weibull distribution: $P_i = i/T_a$ when $i \in [1, T_a\text{-}1]$ and $P_i = 0.997$ when $i = T_a$, as shown in Fig. 10(a). In this way, a group of S_a is created that is scattered in a certain band and concentrated around the peak of the probability density function (PDF).

Step2: The collection of the local strength $S_b(j)$ for the j^{th} dependent crack is shifted to the decreasing part of the PDF, as shown in Fig. 10(b), because the local region where dependent cracks initiate generally has a higher initial fatigue resistance to cracking than that of independent cracks. $S_b(j)$ are then selected at the cumulative probability level $P_j = j\times(1\text{-}P_{peak})/(T_b + 1)$ ($j \in [1, T_b]$), where P_{peak} is the cumulative probability at the peak of the PDF. Consequently, a set of S_b is generated to represent the local strengths at which dependent cracks initiate.

Step3: Provided local strength collections for both independent cracks and dependent cracks are available, the j^{th} dependent crack with a local strength $S_b(j)$ can be matched to an independent crack with a local strength $S_a(i)$. $S_a(i)$ should be less than $S_b(j)$, considering that the independent crack initiates earlier than the dependent crack in an interactive region. After matching with a dependent crack, $S_a(i)$ is removed from the set of S_a to avoid an independent crack interacting with multiple dependent cracks.

Step4: Since the local strength for independent and dependent cracks in an interactive region is known, the range of crack spacing $[d_{min}, d_{max}]$ between two cracks should be determined. Here, d_{max} is equal to the critical crack spacing of 2.25 mm, while d_{min} is initially set at 0.05 mm as the minimum crack spacing observed in fatigue tests. Given a pair of $S_a(i)$ and $S_b(j)$, d_{min} should be recalibrated to avoid the fatigue cycles for dependent crack initiation exceeding an expected limit.

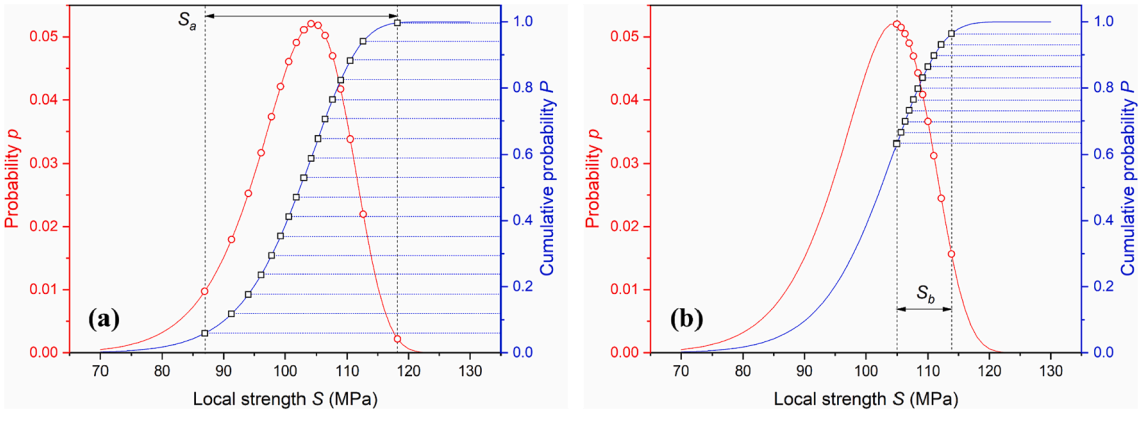

Fig. 10. Collections of local strength for independent cracks (a) and dependent cracks (b), given a statistical distribution of local strength.

Step5: Considering the spatial randomness of transverse matrix cracks presented in [11], the matching of local strengths for a pair of independent and dependent cracks (Step 3) and the determination of the crack spacing (Step 4), are assumed to be a random process. Therefore, given a local strength $S_b(j)$ for the j^{th} dependent crack, 100 times Monte Carlo simulations are performed to obtain a $S_a(i)$ and d in the bounded domains.

3.2.3. Fatigue life of dependent crack initiation

As the local strength and distance about independent and dependent cracks can be determined, the number of fatigue cycles for a dependent crack initiation is further investigated. In an interactive region, the local position of the dependent crack at 90 plies experiences a stress redistribution where the maximum cyclic stress is represented as two consecutive blocks under stress levels of σ_{p1} and σ_{p2} (see Fig. 11).

Prior to the independent crack initiation, the maximum stress at this local position remains constant and is equal to the applied maximum stress applied to the 90 plies, denoted as σ_{p1}. The fatigue cycles consumed n_1 under σ_{p1} is therefore equal to the fatigue life of the independent crack initiation N_a. Once the independent crack initiates, this maximum stress is redistributed, and can be calculated by:

$$\sigma_{p2} = a_0 - a_1 \times a_2{}^d \tag{4}$$

Eq.(4) is obtained from the finite element model presented in Section 2.3.1. The fitted parameters a_0, a_1, a_2 are listed in Table 3 for different stress levels, where d is the distance of this local position from the independent crack.

The consumed fatigue cycles n_2, under σ_{p2}, can be derived based on a strength-based failure criterion that the residual strength σ_r of the local position should decrease to σ_{p2} when the dependent crack initiates. Therefore, the Broutman-Sahu model is adopted here to calculate the residual strength of this local position, as expressed by Eq.(5).

$$\sigma_r = \sigma_{ult} - \sum_i \left(\sigma_{ult} - \sigma_{pi}\right) \frac{n_i}{N_i} \tag{5}$$

where σ_{ult} is the local strength; n_i is the fatigue cycles consumed at the applied stress level σ_{pi}; N_i is the failure life of this local position at a constant stress level σ_{pi}, and can be calculated from Eq.(2) and Eq.(3). The reason for using the Broutman-Sahu model here is that it omits the additional residual strength tests. Based on this residual strength model, the associated fatigue cycles n_2 consumed under the redistributed stress σ_{p2} (see Fig. 11), as calculated from 100 times Monte Carlo simulations (Step 5 in Section 3.2.2.), were averaged and then summed with n_1 to obtain the fatigue cycles consumed for a dependent crack initiation at this interactive region.

Overall, the prediction of the number of cracks with increasing number of fatigue cycles shown in Fig. 9 should be improved to take into account the interaction among cracks. For each statistical distribution of local strengths shown in Fig. 7(b), the interactive region and associated fatigue cycles of dependent crack initiation can be determined by the above steps. The number of transverse matrix cracks, including both independent and dependent cracks, as the number of fatigue cycles increases can then be updated from the results shown in Fig. 9. Based on the gauge length of 80 mm, which corresponds to the damage monitoring area during the tests, the updated crack number can be converted to crack density. Fig. 12 shows two sets of crack density evolution with increasing number of fatigue cycles from both the modelling (area plots) and experiments (dot plots) at the stress levels of 70% and 63% of UTS. As observed, the modelled scatter range covers the most of the experimental data. The negative correlation between crack density and the number of fatigue cycles consumed at the saturation is also achieved by the model. Therefore, the empirical parameters involved in the model and the proposed modelling strategy are suitable to describe the scattering phenomena of crack evolution.

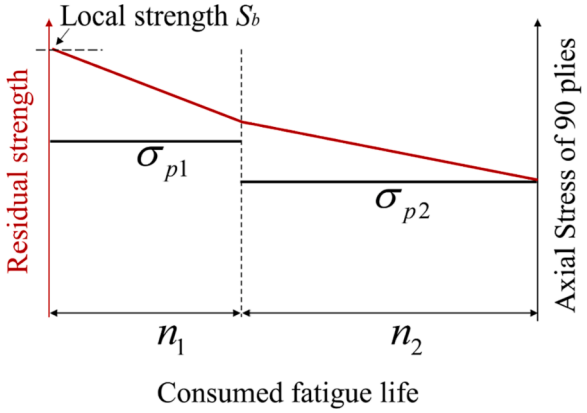

Fig. 11. Variations of axial stress and the degradation of residual strength at the local region of 90 plies before the initiation of a dependent crack.

Table 3
The fitted parameters in the function of axial stress state at the cracked region of 90 plies for different stress levels.

Stress level	a_0 (MPa)	a_1 (MPa)	a_2 (mm^{-1})
74% of UTS	91.3933	86.3079	0.1660
70% of UTS	86.8237	81.9925	
66% of UTS	82.2540	77.6771	
63% of UTS	77.6843	73.3617	

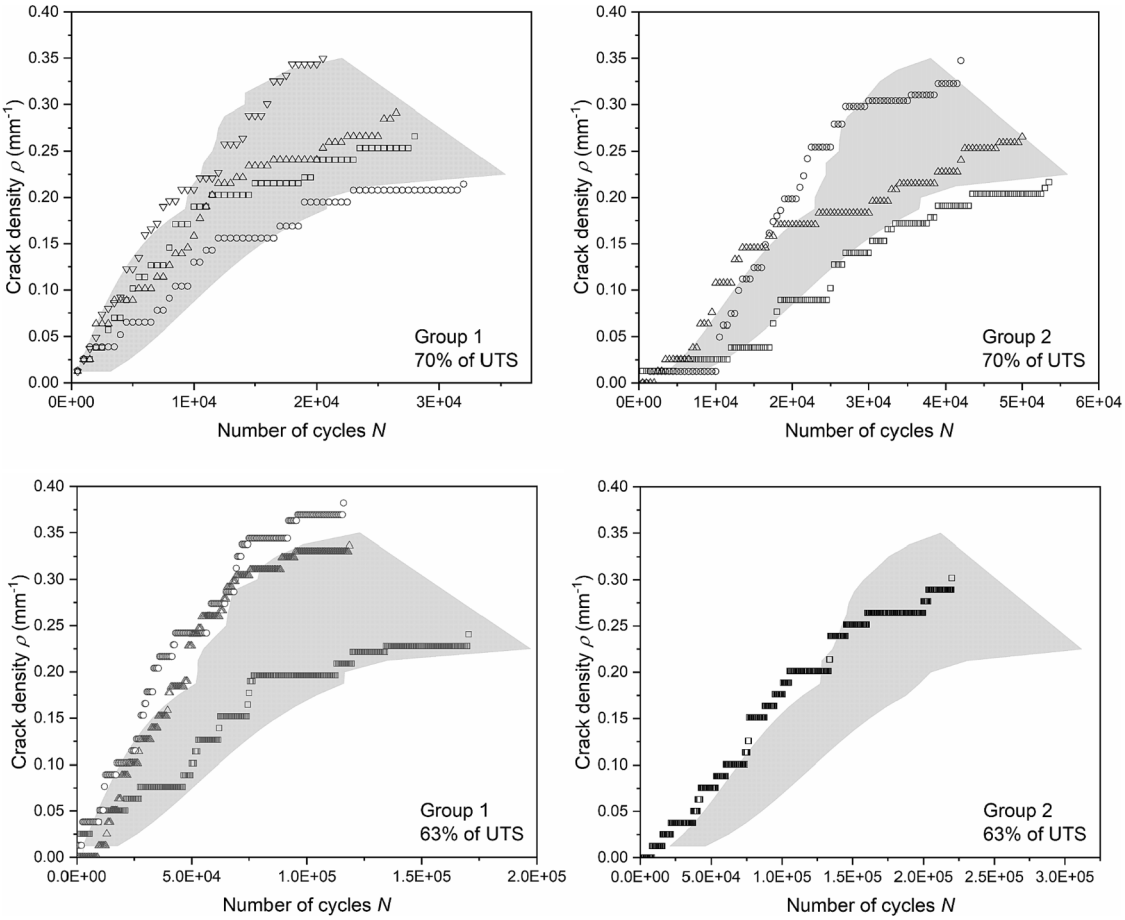

Fig. 12. Comparisons between the experimental results (dot plots) and modelling results (area plots) about the evolution of crack density for the two groups of specimens under stress levels at 70% and 63% of UTS.

3.3. Validation

To further check the applicability of the proposed model, stress levels at 74% and 66% of UTS, which are not included in the data input for the model calibration, are selected here. Fig. 13 shows both modelling results (area plots) and test data (dot plots) for the evolution of crack density as the number of cycles increases. As can be seen, the modelled scatter appears to be less qualified than that in Fig. 12. Compared to Group 2, more test data is covered in the modelled scatter plot for Group 1. These results could be attributed to the availability of more data from Group 1 specimens than that Group 2 specimens during the model calibration. Despite some discrepancy between modelling and testing in terms of crack evolution history, the model captures a reasonable scatter range of saturated crack density and the predicted error in the fatigue life limits at crack saturation is less than 15%. Therefore, the modelling results are in acceptable agreement with the test data, indicating that the proposed model can provide guidance for experimental design and probabilistic analysis under different stress levels.

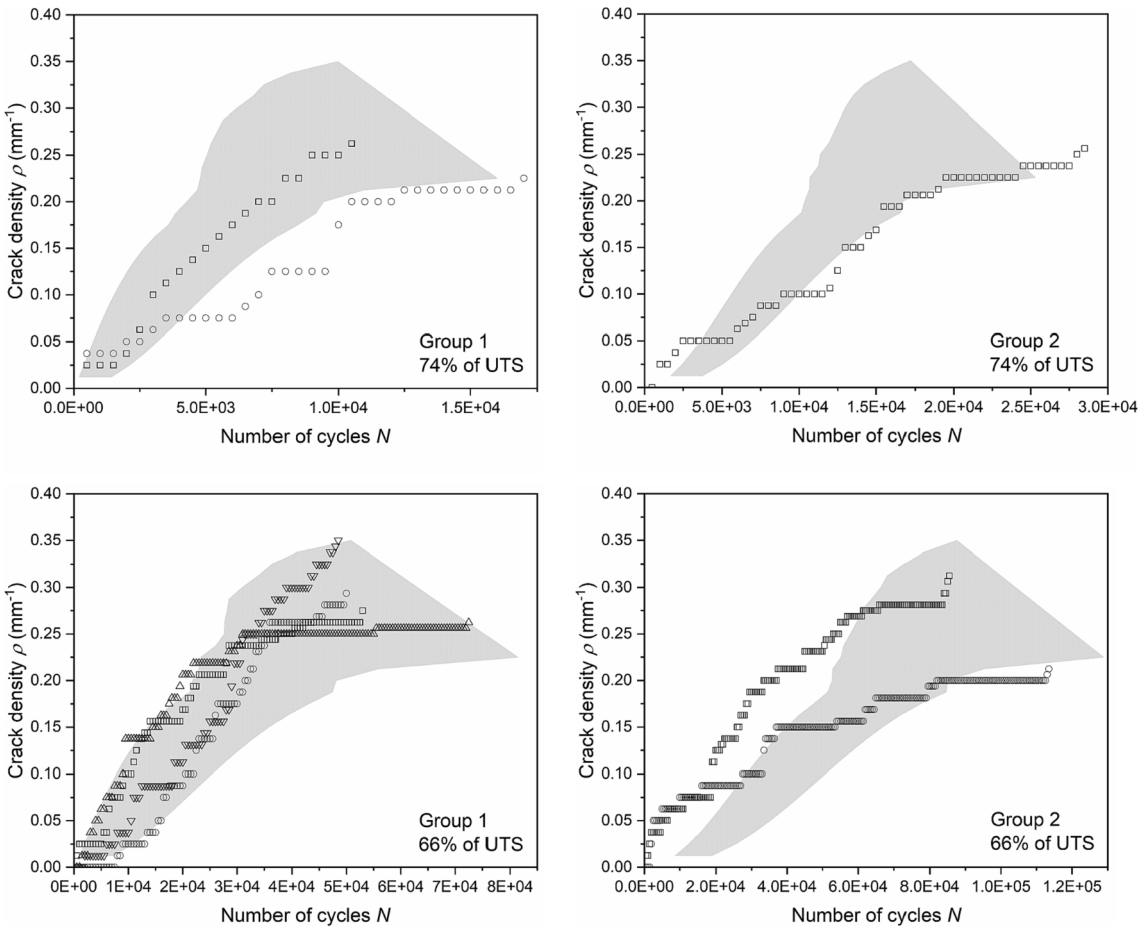

Fig. 13. Comparisons between the experimental results (scatter plots) and modelling results (area plots) about the evolution of crack density for the two groups of specimens under stress levels at 74% and 66% of UTS.

4. Discussion

In the model, given a local strength distribution of 90 plies, the severity of interaction among cracks and the fatigue cycles for crack initiation can be determined according to the local strength distribution-dependent crack ratio relationship and the local strength-fatigue life relationship calibrated from test data. Therefore, the statistical distributions of local strengths generated in Fig. 7(b) behave as the scatter input to the model to produce the variation in crack evolution among specimens. The agreement between the model and test data on the scatter range of crack evolution (see Fig. 12 and Fig. 13) indicates that the simulated scatter input (local strength distribution of 90 plies) is reasonable to quantify the initial fatigue resistance to cracking and to describe the stochastic crack evolution with increasing number of fatigue cycles among specimens. When moving to high frequency and high stress ratio load conditions, the model should take into account other fatigue-induced factors such as cyclic creep and hysteresis heat, which could become significant in affecting the fatigue crack resistance [45–48]. Overall, the hypothesis proposed in Section 1, that local strength variations can be considered as the dominant scattering source to control the fatigue life for crack initiation at 90 plies among specimens, is verified by the present analysis performed under low frequency (5 Hz) and stress ratio (R = 0.1) from both modelling and experimental perspectives. Furthermore, by introducing the relationship between the local strength distribution and the dependent crack ratio, the present model implicitly takes into account the level of interaction between transverse matrix cracks and delamination: specimens with high dependent crack ratios usually show less delamination propagation and vice versa.

As the local strength distribution of 90 plies is the dominant source of scatter here, the approach to relate the local strength to fatigue cycles for the independent crack initiation becomes a key point of the model. The local strength refers to the initial fatigue strength, and it can be related to the in-situ strength of 90 plies obtained from static tests. The question then becomes how to obtain the relationship between static strength and fatigue life. Since both static strength and fatigue life for a local region of 90 plies cannot be obtained experimentally at the same time, this relationship is difficult to derive. As a result, the Strength Life Equal Rank Assumption (SLERA) used in Section 3.1.2. is not easy to prove. D'Amore and Grassia [27] suggested that the SLERA can be applied if the scatter of the fatigue life is mainly dominated by the scatter of the static strength and other sources of scatter induced during the fatigue tests remain negligible. As a final note, it would be useful to find out how to verify this assumption and to fully identify the loading

conditions under which it may be valid.

5. Conclusions

In this present work, the stochastic evolution of transverse matrix cracks was monitored in situ for CFRP cross-ply laminates subjected to tension–tension fatigue loading at different stress levels. Then, a critical crack spacing was obtained by finite element modelling to verify the interaction among transverse matrix cracks. Finally, a probabilistic model was developed and validated with test data to investigate the stochastic nature of crack evolution among specimens. The main conclusions are as follows:

1) The proposed probabilistic model can describe the scattering region of the transverse matrix crack evolution for loading cases with low fatigue test frequency (5 Hz) and stress ratio (R = 0.1).
2) The variation in local strengths at 90 plies is the dominant source of scatter among specimens during fatigue testing, which governs the initial fatigue resistance to cracking and determines the accumulation of transverse matrix cracks.
3) The dependent crack ratio can be used to quantify not only the severity of the interaction between independent and dependent cracks but also the level of interaction between transverse matrix cracks and delamination.

The modelling strategy proposed in the current work, by considering the independent and dependent crack evolution separately, can be used to predict the evolution of tunnel cracking of other cross-ply configurations and materials under fatigue loading. In this way, more physical phenomena observed in experiments can be considered during the modelling of crack evolution under fatigue loading. Due to a relatively thick 90 block of the cross-ply laminates used in the present work, a small number of dependent cracks occurred during fatigue testing, so a one-time interaction between independent and dependent cracks is considered in the proposed model. However, for cross-ply laminates with different 90 block/ply and materials, the model should be updated to consider the possible multiple-time interaction among cracks for a wider application.

Declaration of Competing Interest

The authors declare that they have no known competing financial interests or personal relationships that could have appeared to influence the work reported in this paper.

Data availability

The test data required to reproduce the above findings are available to download via the 4TU.ResearchData repository at https://data.4tu.nl/articles/_/12927974.

Acknowledgements

The authors would like to thank the financial supports of China Scholarship Council (No.201706290028).

References

[1] R.C. Alderliesten, Critical review on the assessment of fatigue and fracture in composite materials and structures, Eng. Fail. Anal. 35 (2013) 370–379, https://doi.org/10.1016/j.engfailanal.2013.03.022.
[2] D. Ma, P. Verleysen, S. Chandran, M. Giglio, A. Manes, A modified peridynamic method to model the fracture behaviour of nanocomposites, Eng. Fract. Mech. 247 (2021), 107614, https://doi.org/10.1016/j.engfracmech.2021.107614.
[3] X. Li, J. Kupski, S. Teixeira De Freitas, R. Benedictus, D. Zarouchas, Unfolding the early fatigue damage process for CFRP cross-ply laminates, Int. J. Fatigue (2020) 140, https://doi.org/10.1016/j.ijfatigue.2020.105820.
[4] K.L. Reifsnider, R. Jamison, Fracture of fatigue-loaded composite laminates, Int. J. Fatigue 4 (1982) 187–197, https://doi.org/10.1016/0142-1123(82)90001-9.
[5] H. Pakdel, B. Mohammadi, Stiffness degradation of composite laminates due to matrix cracking and induced delamination during tension-tension fatigue, Eng. Fract. Mech. 216 (2019), 106489, https://doi.org/10.1016/j.engfracmech.2019.106489.
[6] J.A. Glud, J.M. Dulieu-Barton, O.T. Thomsen, L.C.T. Overgaard, Fatigue damage evolution in GFRP laminates with constrained off-axis plies, Compos. A Appl. Sci. Manuf. 95 (2017) 359–369, https://doi.org/10.1016/j.compositesa.2017.02.005.
[7] H. Pakdel, B. Mohammadi, Characteristic damage state of symmetric laminates subject to uniaxial monotonic-fatigue loading, Eng. Fract. Mech. 199 (2018) 86–100, https://doi.org/10.1016/j.engfracmech.2018.05.007.
[8] M. Saeedifar, H. Hosseini, The Effect of Interlaminar and Intralaminar Damage Mechanisms on the Quasi - Static Indentation Strength of Composite Laminates, Appl. Compos. Mater. (2023), https://doi.org/10.1007/s10443-023-10123-x.
[9] J. Wang, T. Qin, N. Rao, Y. Li, M. Heidari-Rarani, K. Schröder, Three-dimensional progressive damage and failure analysis of double-lap composite bolted joints under quasi-static tensile loading, Compos. Struct. 285 (2022), 115227, https://doi.org/10.1016/j.compstruct.2022.115227.
[10] M.A. Jebeli, M. Heidari-Rarani, Development of Abaqus WCM plugin for progressive failure analysis of type IV composite pressure vessels based on Puck failure criterion, Eng. Fail. Anal. 131 (2022), 105851, https://doi.org/10.1016/j.engfailanal.2021.105851.
[11] X. Li, M. Saeedifar, R. Benedictus, D. Zarouchas, Damage accumulation analysis of CFRP cross-ply laminates under different tensile loading rates, Composites Part C (2020) 000, https://doi.org/10.1016/j.jcomc.2020.100005.
[12] M. Mehdikhani, N.A. Petrov, I. Straumit, A.R. Melro, S.V. Lomov, L. Gorbatikh, The effect of voids on matrix cracking in composite laminates as revealed by combined computations at the micro- and meso-scales, Compos. A 117 (2019) 180–192, https://doi.org/10.1016/j.compositesa.2018.11.009.
[13] S. Koley, P.M. Mohite, C.S. Upadhyay, A micromechanical study and uncertainty quantification for effective properties of unidirectional fibre reinforced composites, Compos. Struct. (2019) 225, https://doi.org/10.1016/j.compstruct.2019.111141.
[14] J.-M. Berthelot, J.-F. Le Corre, Statistical analysis of the progression of transverse cracking and delamination in cross-ply laminates, Composite Science and Technology 60 (2000) 2659–2669, https://doi.org/10.1016/S0266-3538(00)00140-8.

[15] L. Maragoni, P.A. Carraro, M. Quaresimin, Effect of voids on the crack formation in a [45/-45/0]s laminate under cyclic axial tension, Compos. A 91 (2016) 493–500, https://doi.org/10.1016/j.compositesa.2016.02.018.
[16] D. Ma, S. Campos Amico, M. Giglio, A. Manes, Effect of fibre bundle uncertainty on the tensile and shear behaviour of plain-woven composites, Compos. Struct. 259 (2021), 113440, https://doi.org/10.1016/j.compstruct.2020.113440.
[17] D. Ma, M. Giglio, A. Manes, Numerical investigation on the uniaxial compressive behaviour of an epoxy resin and a nanocomposite, Eur. J. Mech. A/Solids 92 (2022), 104500, https://doi.org/10.1016/j.euromechsol.2021.104500.
[18] J. Gao, Y. Yuan, Probabilistic modeling of stiffness degradation for fiber reinforced polymer under fatigue loading, Eng. Fail. Anal. 116 (2020), 104733, https://doi.org/10.1016/j.engfailanal.2020.104733.
[19] J. Gao, P. Zhu, Y. Yuan, Z. Wu, R. Xu, Strength and stiffness degradation modeling and fatigue life prediction of composite materials based on a unified fatigue damage model, Eng. Fail. Anal. 137 (2022), 106290, https://doi.org/10.1016/j.engfailanal.2022.106290.
[20] Y. Huang, J. Varna, R. Talreja, Statistical methodology for assessing manufacturing quality related to transverse cracking in cross ply laminates, Compos. Sci. Technol. 95 (2014) 100–106, https://doi.org/10.1016/j.compscitech.2014.02.010.
[21] J. Montesano, C.V. Singh, Predicting evolution of ply cracks in composite laminates subjected to biaxial loading, Compos. B Eng. 75 (2015) 264–273, https://doi.org/10.1016/j.compositesb.2015.01.039.
[22] J.-M. Berthelot, A. Ei Mahi, J.-F. Le Corre, Development of transverse cracking in cross-ply laminates during fatigue tests, Compos. Sci. Technol. 61 (2001) 1711–1721, https://doi.org/10.1016/S0266-3538(01)00068-9.
[23] N. Jagannathan, S. Gururaja, C.M. Manjunatha, Probabilistic strength based matrix crack evolution model in multi-directional composite lamiantes under fatigue loading, Int. J. Fatigue 117 (2018) 135–147, https://doi.org/10.1016/j.ijfatigue.2018.08.016.
[24] K.H. Ben, Z. Ayadi, F. Edgren, A. Pupurs, J. Varna, Statistical model for initiation governed intralaminar cracking in composite laminates during tensile quasi-static and cyclic tests, Int. J. Fatigue 116 (2018) 1–12, https://doi.org/10.1016/j.ijfatigue.2018.05.030.
[25] P. Chou, R. Croman, Residual Strength in Fatigue Based on the Strength-Life Equal Rank Assumption*, J. Compos. Mater. 12 (1978) 177, https://doi.org/10.1177/002199837801200206.
[26] V.A. Passipoularidis, T.P. Philippidis, Strength Degradation due to Fatigue in Fiber Dominated Glass/Epoxy Composites: A Statistical Approach, J. Compos. Mater. (2009) 43, https://doi.org/10.1177/0021998308097738.
[27] A. D'Amore, L. Grassia, Principal Features of Fatigue and Residual Strength of Composite Materials Subjected to Constant Amplitude (CA) Loading, Materials 12 (2019) 2586, https://doi.org/10.3390/ma12162586.
[28] H.T. Hahn, R.Y. Kim, Proof Testing of Composite Materials, J. Compos. Mater. 9 (1975) 297, https://doi.org/10.1177/002199837500900308.
[29] A. D'Amore, L. Grassia, A method to predict the fatigue life and the residual strength of composite materials subjected to variable amplitude (VA) loadings, Compos. Struct. 228 (2019), 111338, https://doi.org/10.1016/j.compstruct.2019.111338.
[30] G. Sendeckyj, Fitting Models to Composite Materials Fatigue Data, ASTM International (1981) 245–260, https://doi.org/10.1520/stp29314s.
[31] P.A. Carraro, L. Maragoni, M. Quaresimin, Prediction of the crack density evolution in multidirectional laminates under fatigue loadings, Compos. Sci. Technol. 145 (2017) 24–39, https://doi.org/10.1016/j.compscitech.2017.03.013.
[32] V.R.P. Gabriel, M.S. Loukil, J. Varna, Intralaminar cracking during cyclic loading in laminates with distributed failure stress in 90-plies, Int. J. Fatigue 161 (2022), 106909, https://doi.org/10.1016/j.ijfatigue.2022.106909.
[33] T.P. Philippidis, V.A. Passipoularidis, Residual strength after fatigue in composites : Theory vs, experiment. International Journalof Fatigue 29 (2007) 2104–2116, https://doi.org/10.1016/j.ijfatigue.2007.01.019.
[34] D. Garoz, M. Hajikazemi, T.D. Dinh, P.W. Van, Mesoscale finite element analysis of cracked composite laminates under out- of-plane loads using 3D periodic boundary conditions, Compos. Struct. 235 (2020), 111699, https://doi.org/10.1016/j.compstruct.2019.111699.
[35] F. Teimouri, M. Heidari-Rarani, A.F. Haji, Finite element modeling of mode I fatigue delamination growth in composites under large-scale fiber bridging, Compos. Struct. 263 (2021) 11376, https://doi.org/10.1016/j.compstruct.2021.113716.
[36] S. Karimi, F.H. Aboutalebi, M. Heidari-Rarani, Developments in remeshing-free fatigue crack growth simulation including a new adaptive virtual crack closure technique, Fatigue Fract. Eng. Mater. Struct. 45 (2022) 2293–2312, https://doi.org/10.1111/ffe.13735.
[37] B.R. Pathakokila, R. Koona, R.K. Avasarala, S.D. Ambadipudi, V. Manoj Kumar Uppuluri, Statistical analysis for fatigue life evaluation of woven E-glass/epoxy composite laminates containing off-centre interacting circular holes, Mechanics of Time-Dependent Materials 25 (2021) 327–340, https://doi.org/10.1007/s11043-020-09444-2.
[38] Hexcel. HexPly ® 6376 - Product Data Sheet - 2016 EU Version 1 2.
[39] X. Li, R. Benedictus, D. Zarouchas, Early Fatigue Damage Accumulation of CFRP Cross-Ply Laminates Considering Size and Stress Level Effects, Int. J. Fatigue 159 (2022), 106811.
[40] J.A. Glud, J.M. Dulieu-Barton, O.T. Thomsen, L.C.T. Overgaard, Automated counting of off-axis tunnelling cracks using digital image processing, Compos. Sci. Technol. 125 (2016) 80–89, https://doi.org/10.1016/j.compscitech.2016.01.019.
[41] P.A. Carraro, L. Maragoni, M. Quaresimin, Characterisation and analysis of transverse crack-induced delamination in cross-ply composite laminates under fatigue loadings, Int. J. Fatigue 129 (2019), 105217, https://doi.org/10.1016/j.ijfatigue.2019.105217.
[42] D. Ma, X. Li, A. Manes, Y. Li, Numerical modelling of ice: Mechanical behaviour of ice under high strain rates, Int. J. Impact Eng (2023) 172, https://doi.org/10.1016/j.ijimpeng.2022.104375.
[43] M. Quaresimin, P.A. Carraro, L.P. Mikkelsen, N. Lucato, L. Vivian, P. Brøndsted, et al., Damage evolution under cyclic multiaxial stress state: A comparative analysis between glass/epoxy laminates and tubes, Compos. B 61 (2014) 282–290, https://doi.org/10.1016/j.compositesb.2014.01.056.
[44] Abaqus. User Documentation 2017 Dassault Systemes Simulia Corp.
[45] R. Růžek, M. Kadlec, L. Petrusová, Effect of fatigue loading rate on lifespan and temperature of tailored blank C/PPS thermoplastic composite, Int. J. Fatigue 113 (2018) 253–263, https://doi.org/10.1016/j.ijfatigue.2018.04.023.
[46] A.V. Movahedi-Rad, T. Keller, A.P. Vassilopoulos, Creep effects on tension-tension fatigue behavior of angle-ply GFRP composite laminates, Int. J. Fatigue 123 (2019) 144–156, https://doi.org/10.1016/j.ijfatigue.2019.02.010.
[47] A.V. Movahedi-Rad, T. Keller, A.P. Vassilopoulos, Stress ratio effect on tension-tension fatigue behavior of angle-ply GFRP laminates, Int. J. Fatigue 126 (2019) 103–111, https://doi.org/10.1016/j.ijfatigue.2019.04.037.
[48] M. Eftekhari, A. Fatemi, On the strengthening effect of increasing cycling frequency on fatigue behavior of some polymers and their composites: Experiments and modeling, Int. J. Fatigue 87 (2016) 153–166, https://doi.org/10.1016/j.ijfatigue.2016.01.014.